Nuclear Instruments and Methods in Physics Research A 630 (2011) 22–27

Contents lists available at ScienceDirect

Nuclear Instruments and Methods in Physics Research A

journal homepage: www.elsevier.com/locate/nima

Results from the ARGO-YBJ experiment

S. Vernetto

IFSI-INAF and INFN, Torino, Italy

On behalf of the ARGO-YBJ Collaboration

ARTICLE INFO

Available online 15 June 2010

Keywords:
Gamma ray sources
Blazar
Air shower

ABSTRACT

The full coverage extensive air shower detector ARGO-YBJ, located in Tibet at 4300 m of altitude, has monitored the sky at gamma ray energy $E > 0.6$ TeV in the declination band from -10° to $+70^\circ$. In 424 days the Crab Nebula and Mrk421 have been detected with a significance, respectively, of 7.0 and 8.0 standard deviations.

The analysis of the cosmic ray background in the same sky band, has revealed the existence of a significant excess of the cosmic ray flux in two localized regions of angular size 10°–30°, confirming previous indications. The origin of such excesses is still unexplained.

Concerning the gamma ray sources, the measured spectrum of the Crab Nebula is $dN/dE = (3.7 \pm 0.8) \times 10^{-11} E^{-2.67 \pm 0.25}$ photons cm^{-2} s^{-1} TeV^{-1}, in agreement with other experiments.

During 2008 the observed Mrk421 flux was highly variable, with the strongest flares in March–June, in good correlation with X-ray data. One of the most intense flares occurred in the first half of June and has been deeply studied by different detectors in the energy range from optical to 100 MeV gamma rays, but only partially up to TeV energies, since the moonlight hampered the Cherenkov telescope measurements during the second and most intense part of the emission. Our data complete these observations, with the detection of a signal of intensity of about 7 Crab units on June 11–13, with a statistical significance of 4.2 standard deviations. The observed flux is consistent with a prediction made in the framework of the Synchrotron Self-Compton model, in which the flare is caused by a rapid acceleration of leptons in the jet.

1. The detector

ARGO-YBJ is a full coverage air shower detector located at the Yangbajing Cosmic Ray Laboratory (Tibet, P.R. China, lat 30.1N, long 90.5E, 4300 m a.s.l.). Due to its large field of view (~ 2 sr) and its high duty cycle ($> 90\%$) it can monitor continuously a large fraction of the sky, searching for gamma ray sources at energy $E > 0.6$ TeV.

The apparatus is composed of a central carpet of Resistive Plate Chambers (RPCs) ($\sim 74 \times 78$ m^2, $\sim 93\%$ of active area) enclosed by a guard ring with partial coverage, which allows the extension of the instrumented area up to $\sim 100 \times 110$ m^2. The basic data acquisition element is a cluster (5.7×7.6 m^2), made of 12 RPCs (2.8×1.25 m^2). Each chamber is read by 80 strips of 6.75×61.8 cm^2 (the spatial pixel), logically organized in 10 independent pads of 55.6×61.8 cm^2 which are individually acquired and represent the time pixels of the detector. The full detector is composed of 153 clusters for a total active surface of ~ 6600 m^2 [1].

Operated in *shower mode* ARGO-YBJ records all the events with a number of fired pads $N_{pad} \geq 20$ in the central carpet, detected in a time window of 420 ns. The spatial coordinates and the time of any fired pad are then used to reconstruct the position of the shower core and the arrival direction of the primary particle [2].

The installation of the detector has been completed in autumn 2007 and since November 2007 ARGO-YBJ is in stable data taking with a trigger rate of ~ 3.6 kHz.

2. Sky monitoring

The data used in this analysis have been recorded from 2007 day 311 to 2009 day 89 for a total live time of 424 days. All the events with a zenith angle $\theta < 40^\circ$ and a number of hit pads on the central carpet $N_{pad} \geq 40$ have been considered. The events whose arrival direction determination procedure gives a χ^2 of the fit of the shower front larger than a critical value, have been rejected from the analysis. No gamma/hadron discrimination has been performed on these data.

With the selected events, five sky maps in celestial coordinates are built, for different numbers of hit pads: $N_{pad} \geq 40$, 60, 100, 200,

E-mail address: vernetto@to.infn.it

0168-9002/$ - see front matter © 2010 Elsevier B.V. All rights reserved.
doi:10.1016/j.nima.2010.06.020

300. The maps are produced with the HEALPix (Hierarchical Equal Area isoLatitude Pixelization) package [3]. Each map contains $\sim 3.14 \times 10^6$ pixels of area ~ 0.013 squared degrees. The observed sky covers the declination band from -10° to 70°.

After the evaluation of the background using the *time swapping* method [4], the "event maps" and the "background maps" are integrated over a circular area of radius ψ (whose value depends on the angular resolution), i.e. every bin is filled with the content of all bins whose center has an angular distance less than ψ from its center.

Finally the background map is subtracted to the relative event map, obtaining the "signal map", where for every bin the statistical significance of the excess is calculated.

Fig. 1 shows the sky map for events with $N_{pad} \geq 40$, obtained with a relatively large smoothing radius $\psi = 5^\circ$. The map shows two large hot spots in the region of the galactic anticenter, already reported by the Milagro detector [5].

These regions have been interpreted as excesses of cosmic rays, but the origin is not yet understood. They could be related to the observed large scale anisotropy of cosmic rays propagating in the galactic magnetic field [6,7] or to a galactic nearby source such as a supernova explosion in the recent past [8,9]. The median primary energy E_m corresponding to proton showers with $N_{pad} \geq 40$ (300) is ~ 2 (10) TeV.

The two excesses (>10 standard deviations) are observed around the positions r.a. $\sim 120^\circ$, dec $\sim 40^\circ$ and r.a. $\sim 60^\circ$, dec $\sim -5^\circ$, and correspond to a flux increase of, respectively, $\sim 0.06\%$ and $\sim 0.1\%$.

It is important to note that the deficit regions next to the excesses are due to a known effect of the analysis, which uses also the excess events to evaluate the background, artificially increasing it.

These medium scale excesses affect the point gamma ray source search: if a source is located inside an excess or a deficit region, its significance will be, respectively, overestimated or underestimated. To avoid this normalization procedure described in Ref. [10] is adopted.

Fig. 2 shows the sky map after the correction. For the point like source search, we used the smoothing radius that maximizes the signal to noise ratio, that is $\psi = 1.3^\circ$, 0.7° and 0.5°, respectively, for $N_{pad} \geq 40$, 100 and 300, according to simulations.

The Crab Nebula and Mrk421 are visible with a statistical significance, respectively, of 7.0 and 8.0 standard deviations.

From these data we obtained the Crab energy spectrum $dN/dE = (3.7 \pm 0.8) \times 10^{-11} E^{-2.67 \pm 0.25}$ photons cm^{-2} s^{-1} TeV^{-1}, in fair agreement with previous measurements by HESS [11], MAGIC [12] and Tibet AS-γ [13] (Fig. 3).

As a second step, we analysed the map contents at the positions of several known gamma ray sources. We adopted two gamma ray source catalogues:

(a) the recently published list of bright sources observed by Fermi at $E > 100$ MeV [14];
(b) the TeVCat catalogue, a list of sources seen at $E > 100$ GeV [15].

These catalogues contain, respectively, 115 and 44 sources in the declination band corresponding to the ARGO-YBJ field of view, of which 24 are in common. Merging the two catalogues, we obtained a list of 135 sources, 86 extragalactic and 49 galactic (or unidentified but lying close to the galactic plane). For every source the radius r of the observational window is set to ψ, unless the source is known to be extended. In this case $r = \sqrt{(\psi^2 + \alpha^2)}$ where α is equal to half the angular size.

The median energy E_m corresponding to gamma ray showers with a given number of pads depends on the source spectrum and on the culmination zenith angle. For $N_{pad} \geq 40$ the median energy ranges from ~ 0.6 TeV (for a source culminating at the zenith and with a steep differential spectrum $\propto E^{-3}$) up to ~ 2 TeV (for a source culminating at 20° with a spectrum $\propto E^{-2.5}$).

Fig. 4 shows the statistical significance of the observed sources, excluding the Crab Nebula and Mrk421, for $N_{pad} \geq 40$. No source shows a significance larger than 3 standard deviations (s.d.); however, the mean value of the distribution of the excesses for galactic sources is clearly shifted towards positive values (0.45 ± 0.14) while the mean value for extragalactic sources is compatible with zero (-0.02 ± 0.12).

We found two objects with a significance larger than 3 s.d for $N_{pad} \geq 60$, namely:

(a) MGROJ1908+06 with 3.2 s.d. (discovered by Milagro [16], confirmed by HESS [17] and recently associated to 0FGL J1907.5+0602, a Fermi pulsar [18]);
(b) the unidentified HESS source HESSJ1841-055 [19], with 3.0 s.d.

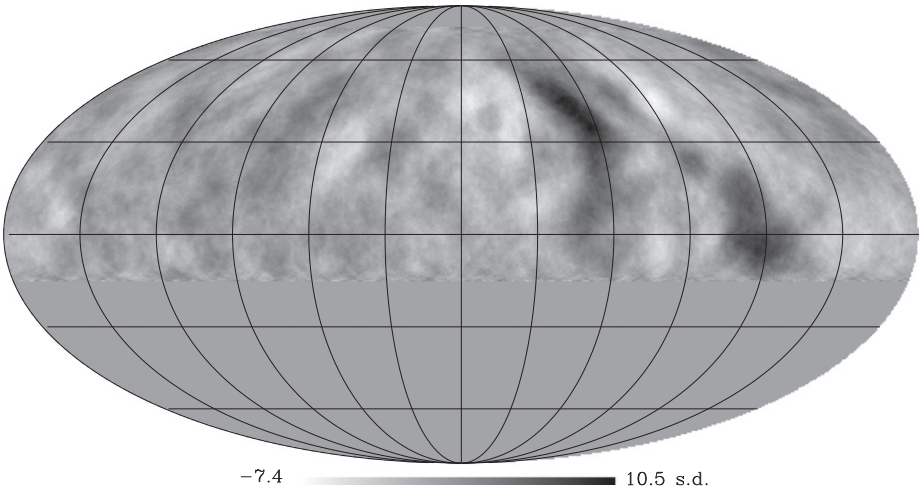

Fig. 1. Sky map in equatorial coordinates obtained in 424 days of measurements, for events with $N_{pad} \geq 40$. The right ascension is zero on the extreme right of the map and increases towards left. The grey scale indicates the statistical significance in standard deviations. The large black spots around the positions r.a. $\sim 120^\circ$, dec $\sim 40^\circ$ and r.a. $\sim 60^\circ$, dec $\sim -5^\circ$ represent two localized excesses in the cosmic ray flux of intensity, respectively, $\sim 0.06\%$ and $\sim 0.1\%$.

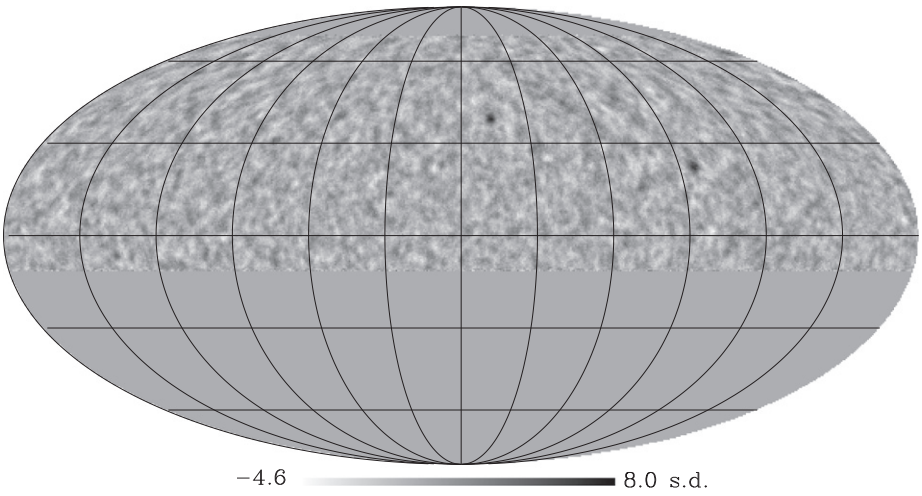

Fig. 2. Sky map after the anisotropy correction, for events with $N_{pad} \geq 40$. The Crab Nebula and Mrk421 are observed with a statistical significance, respectively, of 7.0 and 8.0 standard deviations.

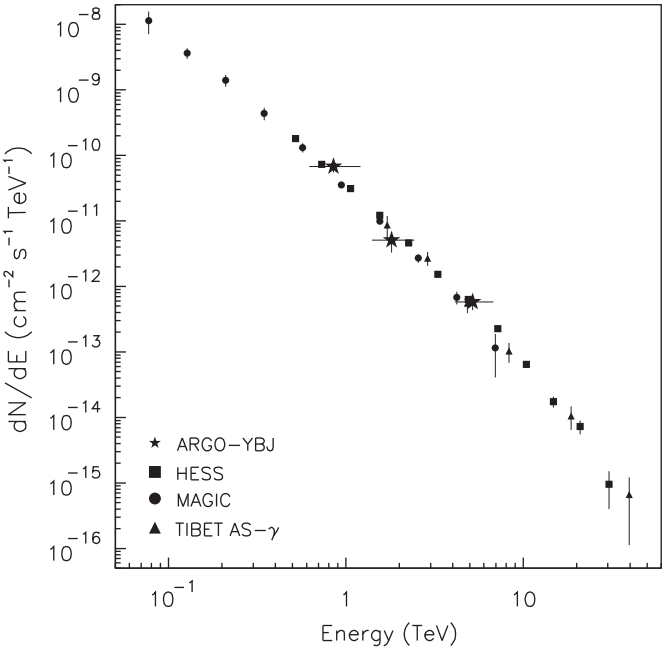

Fig. 3. The Crab Nebula spectrum measured by ARGO-YBJ, compared with other experiments.

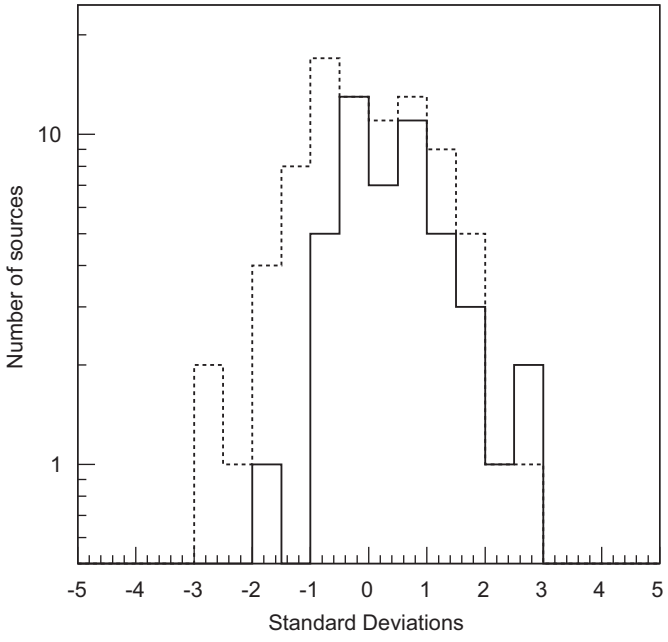

Fig. 4. Distribution of the excesses observed at the positions of 133 gamma ray sources (dashed line: extragalactic sources, solid line: galactic sources).

Considered the number of trials (133 sources $\times 5$ N_{pad} intervals) and the small significance of the excesses it is difficult to say if they are due to gamma rays or to background fluctuations.

3. Observation of Mrk421

During 2008 Mrk421 underwent several flaring episodes, observed at different wavelengths.

The source culminates at the ARGO-YBJ location at a zenith angle $\theta_{culm} = 8.1^{\circ}$, and it is observable every day for 6.38 h with a zenith angle $\theta < 40^{\circ}$. ARGO-YBJ observed Mrk421 from 2007 day 311 to 2008 day 366. The measured gamma ray flux was variable in time, with the largest flares in March–June 2008 [20].

The Mrk421 spectrum has been evaluated from 2008 day 41 to day 180, when the X-ray flux reached the highest levels. In this period (755 observation hours) the signal had a statistical significance of 6.1 standard deviations.

We assumed a power law spectrum $K \times E^{-\alpha}$ multiplied by an exponential factor $e^{-\tau(E)}$ to take into account the absorption of gamma rays in the Extragalactic Background Light (EBL), where the values of $\tau(E)$ are given by Ref. [21].

The spectrum that best fits the data is: $dN/dE = (7.46 \pm 1.70) \times 10^{-11}\, E^{-2.51 \pm 0.29}\, e^{-\tau(E)}$ photons cm^{-2} s^{-1} TeV^{-1}, giving an integral flux above 1 TeV of $4.9 \pm 2.0 \times 10^{-11}$ photons cm^{-2} s^{-1}, about twice that of the Crab Nebula (see Fig. 5).

The gamma ray rate observed by ARGO-YBJ appears to be correlated with the X-ray rate measured by the all sky monitor detector aboard the RXTE satellite in the 1.5–12 keV energy range, as expected from the Synchrotron Self-Compton (SSC) model. Fig. 6 shows the rate of the excess events with $N_{pad} \geq 100$ observed by ARGO-YBJ as a function of time, averaged over 10 days, compared to the corresponding X-ray counting rate of RXTE/ASM [22].

The simultaneous observation of flares at different wavelengths can provide unique information about the source properties and

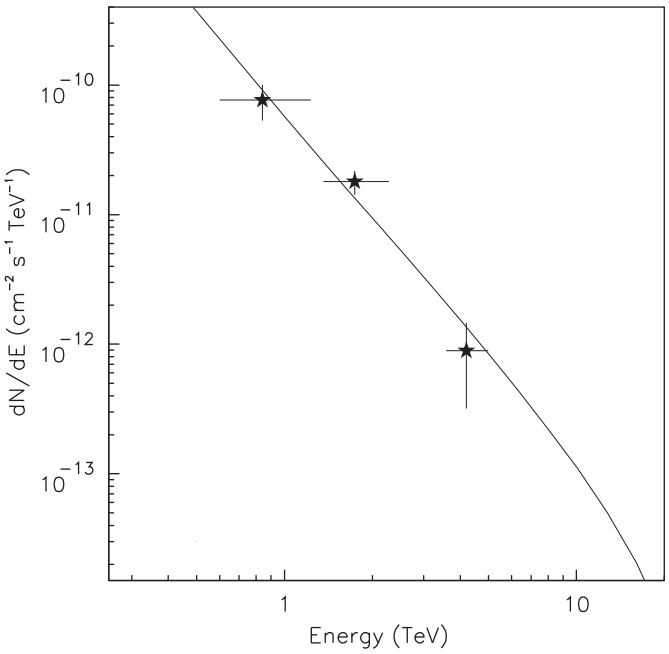

Fig. 5. Mrk421 differential energy spectrum from 2008 day 41 to 180, when the source was in active state. The line represents the best fit to the data.

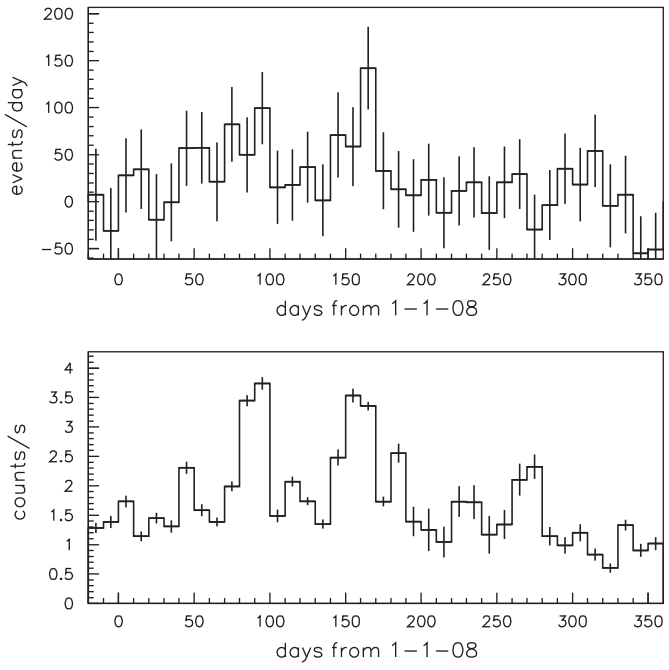

Fig. 6. Upper panel: excess event rate detected from Mrk421 by ARGO-YBJ with $N_{pad} \geq 100$, as a function of time, averaged over 10 days. Lower panel: X-ray counting rate detected by RXTE/ASM, averaged over 10 days.

the radiation processes. A set of simultaneous measurements covering 12 decades of energy, from optical to TeV gamma rays, was performed during the strong flaring activity in the first half of June 2008 by different detectors [23].

In this period two flaring episodes were reported, the first one on June 3–8, observed from optical to TeV gamma rays, the second one, larger and harder, on June 9–15, observed from optical to 100 MeV gamma rays.

Using the multifrequency data, the authors of Ref. [23] derived the spectral energy distribution (SED) for June 6, that shows a typical two humps shape, in agreement with the SSC model. According to the authors, the second hump intensity (that reached a flux of about 3.5 Crab units at energy $E > 400$ GeV) seems to indicate that the variability is due to the hardening/softening of the electron spectrum, and not to the increase/decrease of the electron density.

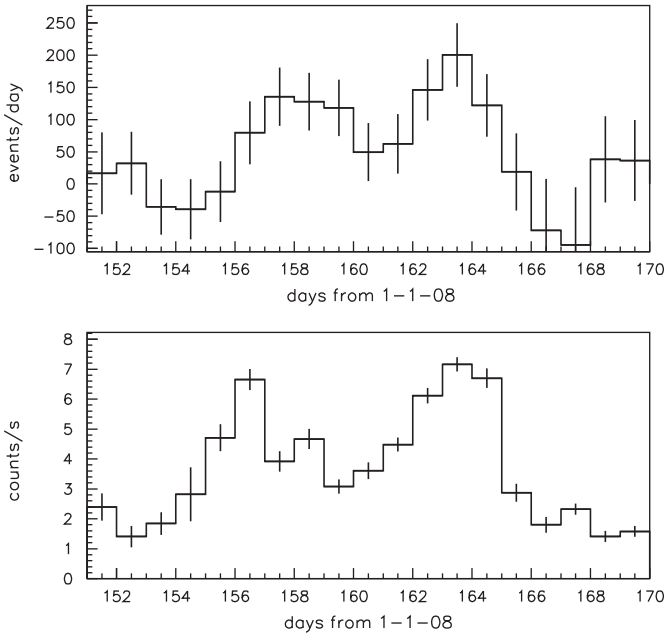

Fig. 7. Mrk421 flare in June 2008. Upper panel: rate of events with $N_{pad} \geq 100$ observed by ARGO-YBJ as a function of time from May 31 00:00 UT to June 19 00:00 UT. Each bin contains the rate averaged over the 3 days interval centered on that bin. Lower panel: daily counting rate of RXTE/ASM.

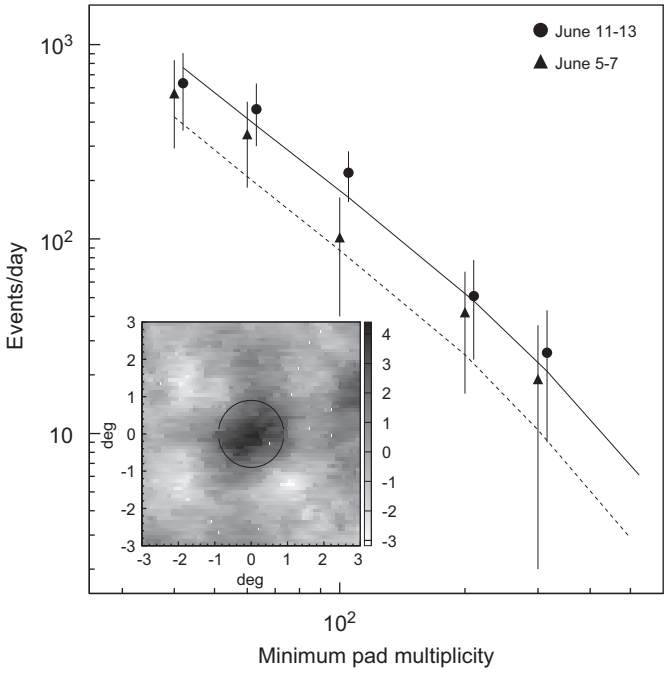

Fig. 8. Event rates observed from Mrk421 by ARGO-YBJ as a function of the event minimum pad multiplicity on June 5–7 and June 11–13 (respectively, triangles and circles). Expected rates according to the model in [23] for the same two periods (respectively, dashed and solid lines). The inset shows the sky map around Mrk421 on June 11–13, for events with $N_{pad} \geq 100$. The grey scale gives the significance of the signal in standard deviations. The circle represents the observational window with radius 0.9°.

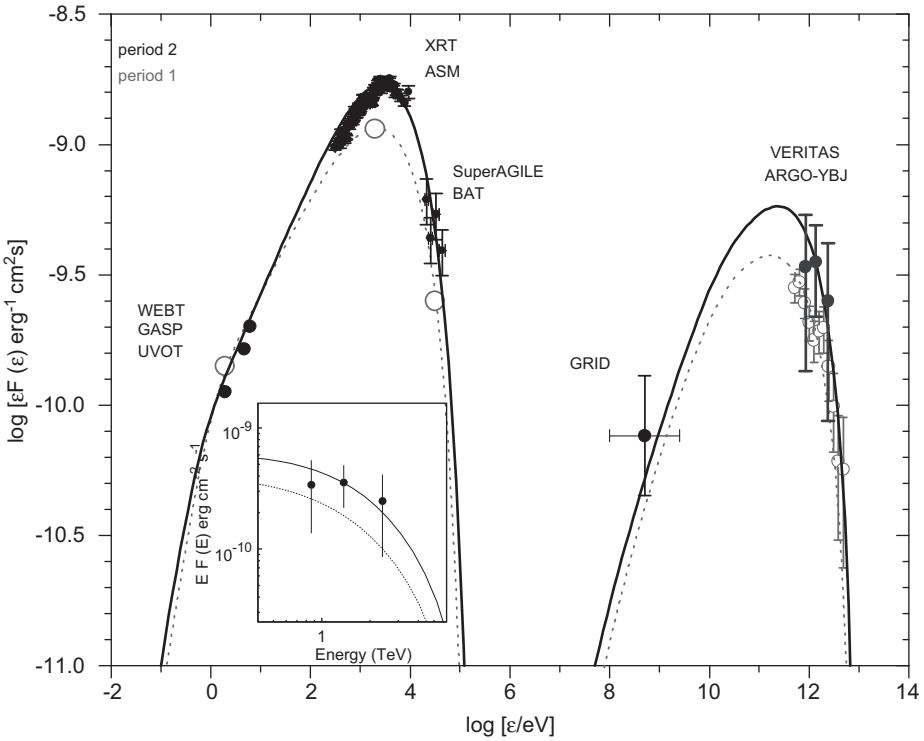

Fig. 9. Mrk421 spectral energy distribution measured by ARGO-YBJ on June 11–13 (large filled circles) together with data of other experiments, obtained during the first flare (open circles), and the second one (filled circles). The curves represent the SEDs modeled in [23] for the first (dashed line) and the second (solid line) flares. The inset shows a zoom on the ARGO-YBJ data.

Their model predicts for the second flare a VHE flux at $E > 1$ TeV of 1.45×10^{-10} photons cm^{-2} s^{-1}, about a factor 2 larger with respect to the first flare, corresponding to about 7 Crab units.

Unfortunately there were no VHE data included in their multiwavelength analysis after June 8 because the moonlight hampered the Cherenkov telescopes measurements. The VHE observation was actually made for such a very important flaring episode by the ARGO-YBJ experiment, that since December 2007 is performing a continuous monitoring of Mrk421.

Since the ARGO-YBJ sensitivity does not allow the observation of a flux of a few Crab units in only one day (i.e. during one transit of the source in the detector field of view), we integrated the measurement over 3 days.

Fig. 7 shows the rate of events with $N_{pad} \geq 100$ observed by ARGO-YBJ during the first half of June, averaged over 3 days, compared with the X-ray flux measured by RXTE/ASM [22]. The source has been detected with a statistical significance of 4.2 standard deviations during the interval 11–13 June, when the maximum of the second flare occurred. The inset of Fig. 8 shows the $6^\circ \times 6^\circ$ sky map around the source position in these 3 days.

Fig. 8 shows the event rate observed by ARGO-YBJ during the two flares compared with the rate expected from a source spectrum given by the theoretical SED, for any N_{pad} interval. The agreement is good.

Finally we estimate the energy spectrum for the second flare (the low significance of the first one does not allow a spectrum evaluation). Fig. 9 gives the measured SED together with all the data in the optical-TeV range, and the theoretical SED for the two flares. The measurements appear in fair agreement with the expected emission.

4. Conclusions

For a period of ~ 15 months ARGO-YBJ monitored the gamma ray sky in the declination band from -10° to $+70^\circ$. The observations of the background have revealed the existence of two regions with size 10°–30°, where the CR flux is enhanced by approximately 0.1%. The origin of these medium scale anisotropies, previously observed by the Milagro experiment, remains unexplained.

A search for point sources of high energy gamma radiation has resulted in the detection with high significance of the Crab Nebula and Mrk421.

Two strong flares from Mrk421 in June 2008 have been observed in a multiwavelength campaign from optical to TeV energies. ARGO-YBJ measured the spectra of Mrk421 above 0.8 TeV during the second flare, completing the multifrequency observations. For the first time an air shower array was able to detect gamma-ray flaring activity at sub-TeV energies on a few days period.

The data acquisition is currently going on with stable detection conditions. Studies to improve the detector sensitivity are in progress, both in the direction of increasing the angular resolution and of rejecting the cosmic ray background, implementing gamma-hadron separation algorithms [24].

References

[1] G. Aielli, et al., Nucl. Instr. and Meth. A 562 (2006) 92.
[2] G. Di Sciascio, et al., in: Proceedings of 30th ICRC, Merida, Mexico, 2007, arXiv:0710.1945.
[3] Gorski, et al., Astrophys. J. 622 (2005) 759 〈http://healpix.jpl.nasa.gov〉.
[4] D.E. Alexandreas, et al., Nucl. Instr. and Meth. A 328 (1993) 570.
[5] A.A. Abdo, et al., Phys. Rev. Lett. 101 (2008) 221101.
[6] J.L. Zhang, et al., in: Proceedings of 31th ICRC, Lodz, Poland, 2009.
[7] M. Amenomori, et al., Science 314 (2006) 439.
[8] L. Drury, F. Aharonian, Astropart. Phys. 29 (2008) 420.
[9] M. Salvati, B. Sacco, Astron. Astrophys. 485 (2) (2008) 527.
[10] S. Vernetto, Z. Guglielmotto, J.L. Zhang, et al., in: Proceedings of 31th ICRC, Lodz, Poland, 2009.
[11] F. Aharonian, et al., Astron. Astrophys. A 457 (2006) 899.
[12] J. Albert, et al., Astrophys. J. 674 (2008) 1037.
[13] M. Amenomori, et al., Astrophys. J. 692 (2009) 61.

[14] A.A. Abdo, et al., 2009, arXiv:0902.134v1.
[15] TeVCat catalogue, 〈http://tevcat.uchicago.edu〉.
[16] A.A. Abdo, et al., Astrophys. J. Lett. 664 (2007) 91.
[17] A. Djannati-Atai, et al., in: Proceedings of 30th ICRC, Merida, Mexico, 2007.
[18] A.A. Abdo, et al., 2009, arXiv:0904.1018v1.
[19] F. Aharonian, et al., Astron. Astrophys. 477 (2008) 353.
[20] S. Vernetto, D. Martello, J.L. Zhang, et al., in: Proceedings of 31th ICRC, Lodz, Poland, 2009.
[21] J.R. Primack, J.S. Bullock, R.S. Sommerville, AIP Conf. Proc. 745 (2005) 23.
[22] RXTE/ASM public data at 〈http://xte.mit.edu/asmlc/ASM.html〉.
[23] I. Donnarumma, et al., Astrophys. J. 691 (2008) L13.
[24] M. Dattoli, et al., in: Proceedings of 31th ICRC, Lodz, Poland, 2009.